

Adaptive Optics Images at 3.5 and 4.8 μm of the Core Arcsec of NGC 1068: More Evidence for a Dusty/Molecular Torus. ^{*}

O. Marco and D. Alloin

European Southern Observatory (ESO), Casilla 19001, Santiago 19, Chile

Submitted to Astronomy & Astrophysics

Abstract. Adaptive optics observations of NGC 1068 have allowed to reach with a 4m class telescope, diffraction-limited images at 3.5 μm (FWHM=0.24") and 4.8 μm (FWHM=0.33") of the central arcsec region. These observations reveal the presence of an unresolved core (radius less than 8 pc at Half Maximum) and an 80 pc sized "disc-like" structure at P.A. $\sim 100^\circ$, which is interpreted as the dusty/molecular torus invoked in the AGN unification scheme. They show as well an extended emission region along the NNE-SSW direction, of 100 pc full size, most probably associated with dust in the NLR. The position of the unresolved core at 3.5 and 4.8 μm is found to be coincident with that of the core observed at 2.2 μm and outlines the location of the central engine in the AGN of NGC 1068. Considering as well previous AO observations at 2.2 μm we infer that there must exist a very steep gradient of the dust grain temperature, close to the central engine. At a distance of 30 pc from the central heating source, the dust grain temperature deduced from the [L-M] color is found to be $\sim 500\text{K}$. The mass of warm dust ($T_{gr} > 500\text{K}$) in the 0.6" diameter core is found to be $\sim 0.5 M_\odot$. The spectral energy distribution from 1 to 10 μm is provided for the 0.6" diameter core. These results are briefly discussed in the context of current torus models.

Key words: Galaxies : NGC 1068 – Galaxies : Seyfert – Galaxies : nuclei – Infrared : galaxies – Galaxies : active – Instrumentation : adaptive optics

1. Introduction

Series of observational facts assembled over the past decade on Active Galactic Nuclei have led to the so-called "unified" model of AGN (for a review of these facts, as well as for the detailed characteristics of the unified

model see Krolik 1999). Our current specific interest in the unified model is that the central engine (black hole and accretion disk) and its close environment (dense gas clouds emitting the broad lines which constitute the broad line region, BLR) are embedded within an optically thick dusty/molecular torus. Along some lines of sight, the torus obscures and even fully hides the central engine and the BLR.

In that respect, the case of NGC 1068, a bright Seyfert 2 active galaxy, is particularly enlightening. The spectrophotometry in polarized light reveals the presence of a hidden BLR (Antonucci & Miller 1985), the conical shape of the narrow line region (NLR) – both on large (Pogge 1988) and small (Evans et al. 1991) scales – indicates that the ionizing radiation is collimated by an opaque blocking torus and, finally, the symmetry center of the UV/optical polarization map (Capetti et al. 1995) is found to be coincident with the radio core (Gallimore et al. 1996a), the 12.4 μm peak (Braatz et al. 1993) and the maser emission (Gallimore et al. 1996b), suggesting that this is the location of the hidden true nucleus.

This object appears then particularly suitable for unveiling the putative torus through its infrared emission, which, according to current models should be quite strong (e.g. Pier & Krolik 1992a, b, 1993; Granato & Danese 1994; Efstathiou, Hough & Young 1995; Granato, Danese & Franceschini 1997). In this search, high spatial resolution is a requisite in order to locate very precisely and to characterize the structure of emission sources. Hence, adaptive optics (hereafter abbreviated AO) in the 1-5 μm window is the tool. At the distance of NGC 1068 (14.4 Mpc), 1" is equivalent to 72 pc (assuming $H_0=75$ km/s/Mpc), allowing to reach a spatial resolution of a few parsecs. Through AO observations, simultaneously in the visible and near-infrared, the 2.2 μm peak emission has already been found to be offset by ~ 0.3 " S of the optical continuum peak as defined by Lynds et al. (1991) and to be coincident with the previously identified "hidden true nucleus" (Marco, Alloin & Beuzit 1997). In the current study, we are presenting new results obtained at 3.5 and 4.8 μm with ADONIS, the AO system working at the ESO

Send offprint requests to: O. Marco

^{*} Based on observations collected at the European Southern Observatory, La Silla, Chile.

Correspondence to: omarco@eso.org

Table 1. Summary of the data sets

filter	λ [μm]	T_{int} [s]	T_{total} [s]	Strehl [%]	visible seeing ["]	airmass
L	3.48	6.0	1152	28	0.7	1.23
M	4.83	1.5	720	36	0.55	1.15
PAH	3.31	60	1440	25	0.66	1.25

3.6 m telescope on La Silla and fully described in Beuzit et al. (1994).

2. Observations and data reduction

The observing run took place from august 13 to 19, 1996, under excellent seeing and transparency conditions (Table 1).

The AO correction was performed on the brightest spot of NGC 1068 in the visible continuum light (Lynds et al. 1991). The wavefront sensor (EBCCD after a red dichroic splitter) has a pixel size of $0.7''$ and takes into account the gravity center of the light within a $6''$ diameter circular entrance. Due to the pixel size of the wavefront sensor, the contribution of the continuum and the lines from the central 50 pc around the Lynds et al. peak (1991) both fall in one pixel: so the contrast is maximum.

The detector was the COMIC camera (Lacombe et al. 1997), at the f/45 Cassegrain focus, which provides an image scale of $0.1''/\text{pixel}$, resulting in a field of view of $12.8'' \times 12.8''$.

NGC 1068 was observed in an imaging mode through the standard spectral L ($3.48 \mu\text{m}$), L' ($3.81 \mu\text{m}$), and M ($4.83 \mu\text{m}$) bands and through a circular variable filter for the PAH (line $3.3 \mu\text{m}$ rest wavelength, and continuum). Through the L, L' and M bands, we observed in a chopping mode, alternating object and sky images by the use of a field selection mirror. We chose an offset of $10''$ to the N and $10''$ to the W.

During the six nights, the visible seeing was measured by the ESO differential image motion monitor. It was excellent during four nights, ranging from $0.4''$ to $0.7''$. Therefore, the efficiency of the AO correction was optimal and the images obtained with COMIC were diffraction-limited. However, the gain of the intensifier was not optimized at that time, which resulted in Strehl ratios lower than expected.

In order to minimize position offsets between the calibration star and the AGN, we selected a reference star within 2 degrees of the target. For both the galaxy and the point spread function (PSF) reference star, the airmass was at most of 1.3, ensuring differential refraction effects to be negligible (less than one pixel).

Individual exposure times were chosen so as to observe under conditions of background limiting performances (BLIP). In this way, the readout-noise is dominated by

the background photon noise, and we just take an average of the images to improve the signal-to-noise ratio. We observed several photometric standard stars to obtain a precise flux calibration and another star to determine the PSF for later deconvolution.

Standard infrared data reduction procedures were applied to each individual frame, for both the galaxy and the reference stars : dead pixel removal, sky subtraction, flat fielding from sky images at each wavelength. As the AO system is compensates for image shifting, no additional shift correction was applied.

Thanks to the length of our observing run, we obtained a largely redundant data set. We discovered in particular that we had experienced a problem of astigmatism during 2 nights, due to an unappropriate tuning of the visible wavefront sensor leading to a very low signal to noise ratio on the Shack-Hartmann analysor (Alloin & Marco 1997). Being aware of this flaw, we decided to review in depth the AO optimization parameters for the entire data set and to remove all suspicious blocks. In addition, we applied a selection procedure of 32-images data cubes, based upon the seeing value and the Strehl ratio. The corresponding equivalent integration times are reported in Table 1.

3. Wavefront analysis sensing

To better interpret the NGC 1068 observations with ADO-NIS, we need to track precisely which visible image of NGC 1068 is seen by the wavefront analysis sensor (WFAS) in its evaluation of the AO correction.

In order to recover this information, we have used HST images with 45 mas pixel size both in the continuum and in the lines (F791W, F547M F658N, and F502N), properly aligned and flux scaled to a same 1 sec exposure at the entrance of the telescope, to construct a composite image which mimics the one seen by the WFAS. The image alignment was performed using point-like sources in the field of view, which allows a registration within 10 mas (Tsetanov, private communication). The flux scaling has included corrections for the exposure time of each image and the mean HST camera efficiency over the corresponding filter. Then, each of these corrected images has been weighted by the corresponding mean WFAS wavelength response, before addition. We find indeed that the light received from NGC 1068 on the WFAS is largely dominated by continuum light and is not much weighted by the [O III] - line light distribution.

And finally, to mimic the image seen on the WFAS CCD, from which the AO corrections are computed, we have degraded the HST composite image by a “seeing” effect of $\sim 1''$: this includes both an atmospheric effect ($\sim 0.6''$ according to the mean seeing value -FWHM- measured on the selected nights of the observing run) and the instrumental spread function ($0.85''$), which is rather large because of the photocathode -CCD spacing. As the WFAS takes into account, to compute the AO correction,

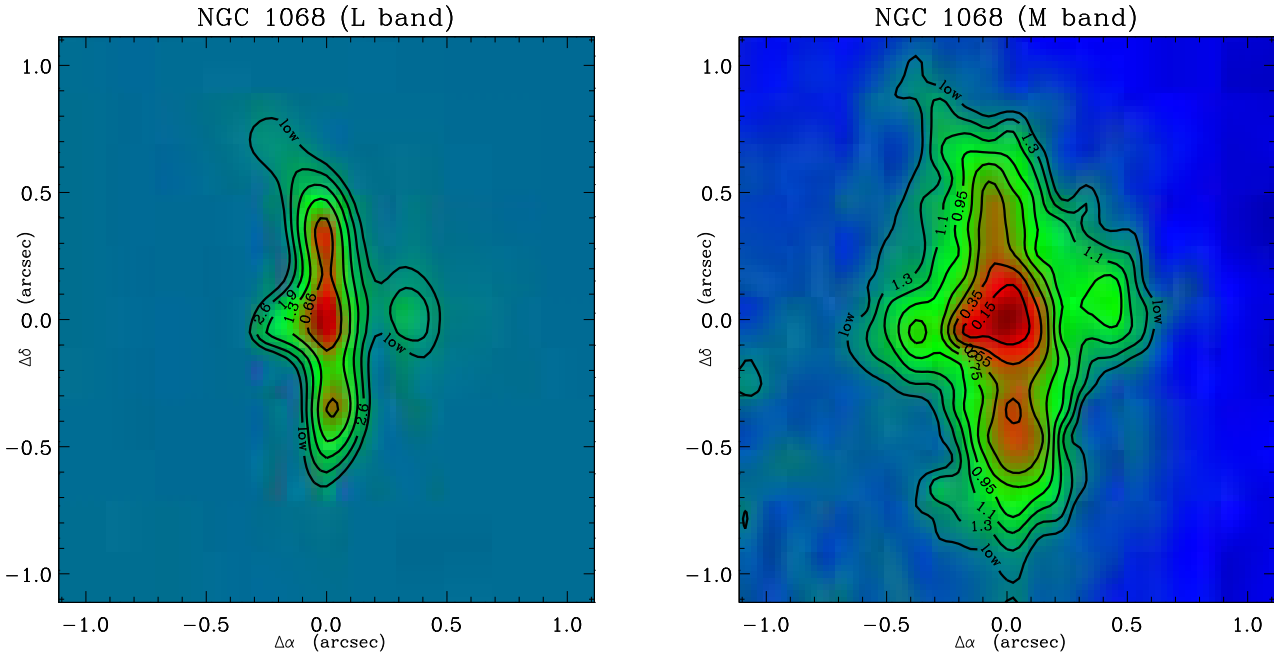


Fig. 1. Left: L band image of NGC 1068. Right: M band image of NGC 1068. North is up, East is to the left.

the light centroid over a $6''$ circular diaphragm, we have derived the light centroid within a $6''$ aperture on the degraded composite HST image. This position is the reference for the WFAS.

We need also to locate the centroid of the degraded HST composite image with respect to the Lynds visible peak, as measured from the HST image F547M. We find a slight offset between the visible centroid and the Lynds visible peak: the visible centroid (using NGC 1068 for the correction) is located 99 mas to the N and 86 mas to the E of the Lynds peak. This offset is taken into account in our estimate of the NGC 1068 infrared sources location (Sect. 4.1). The offset may differ from one AO system to another. In the case of ADONIS, the offset is largely due to the $6''$ entrance to the WFAS.

4. Data analysis

We present in Fig. 1 the L and M band images of NGC 1068. We used a magnitude (log) scale because of the high dynamics of the images provided by the AO. The images have been deconvolved using a Lucy-Richardson algorithm (MIDAS package). We have also observed NGC 1068 in the L' band: this image is very similar to the one obtained in the L band. Thus, our current data analysis and subsequent discussion will be based on the two L and M bands, only.

The L and M band images show:

i) an unresolved core down to the resolution (FWHM) of $0.24''$ (16 pc) and $0.33''$ (22 pc), respectively at 3.5 and $4.8 \mu\text{m}$. This core has already been observed at $3.6 \mu\text{m}$ by Chelli et al. (1987) and at $2.2 \mu\text{m}$ by Marco et al. (1997),

Thatte et al. (1997) and Rouan et al. (1998). The latter give an upper limit of the core size (FWHM) of $0.12''$ (less than 8 pc).

ii) an elongated structure at P.A. $\sim 100^\circ$ particularly prominent in the M band, but also quite well outlined in the L band. This structure is obviously coincident with the structure seen in the K band by Rouan et al. (1998) and is roughly perpendicular to the axis of the inner ionizing cone (P.A. = 15° , Evans et al. 1991). It extends in total over ~ 80 pc, with a bright spot at each of the $\sim E$ and $\sim W$ edges at a radius of ~ 25 pc from the central engine.

iii) an extended emission along the NS direction, almost aligned with the radio axis and the ionizing cone axis. At low level isophotes (in particular in the L band), a change in the direction of the axis of this emission can be noticed, reminiscent of a similar change of direction of the radio jet (Gallimore et al. 1996a).

Down to faint levels, the $4.8 \mu\text{m}$ thermal infrared emission appears to be extended over $\sim 3''$ in diameter (~ 210 pc).

It is striking that the two different AO systems used, ADONIS for the L and M bands and PUEO for the K band, reveal a similar structure of the AGN environment. These AO systems are using WFS of different types, Shack-Hartmann for ADONIS and curvature for PUEO, as well as deformable mirrors of different types, piezo-stack for ADONIS and bimorph for PUEO. The Lucy-Richardson deconvolution applied on both data sets uses PSFs obtained in two different ways: we used an observed stellar PSF in the case of the ADONIS data set – as the L and M band data are less sensitive

Table 2. Photometric data for NGC 1068. Observed fluxes are in Jy.

filter	aperture radius					
	0.3''	0.4''	0.5''	0.6''	0.9''	1.5''
L	0.92	1.34	1.78	2.09	2.76	3.40
M	2.27	3.23	4.41	5.30	7.18	9.73

to rapid PSF fluctuations – and we used the PSF recovered from the AO loop parameters in the case of the PUEO data set. The two AO experiments differ in many aspects, while leading to a similar result for the structure of the AGN dusty environment. Therefore we are quite confident that this structure is real and not hampered by significant AO artifacts (Chapman et al. 1999). Finally it should be noticed that the high resolution image of the AGN in NGC 1068 obtained in the K band with the AO system at the Keck telescope (www2.keck.hawaii.edu/realpublic/ao/ngc1068.html) reveals a comparable structure, pending that a precise orientation and a scale be provided for the Keck AO data set.

4.1. Location of the emission peaks at 3.5 and 4.8 μm and nature of the unresolved core

As it was not possible to observe simultaneously in the visible and in the infrared, we took advantage of a characteristic feature of AO systems which is to preserve the optical center for all objects: the infrared camera field has a position fixed in regard to the centroid of the visible counterpart of the object observed. Indeed, by observing a star (PSF or photometric standard), we determine a reference position in the infrared image to within the precision we are aiming at in this study (better than one infrared camera pixel, $0.1''$). Any offset of the galaxy infrared peak relatively to the star infrared peak would then reveal an intrinsic offset between the galaxy infrared light peak and the galaxy visible light peak. This is a method for positioning infrared versus visible sources in the AGN.

To improve the precision, we have fitted the PSF and the NGC 1068 emission peaks by Gaussian profiles. The L and M band peaks in NGC 1068 are coincident within the positional precision given above. We have also derived the position of this L and M peak in NGC 1068 with respect to the visible peak, following the procedure described in Sect. 3: it is offset by $0.3 \pm 0.05''$ S and $0.1 \pm 0.05''$ W of the visible continuum peak and therefore is found to be coincident with the K band emission peak (Marco et al. 1997), within the error bars.

Therefore, the compact core at 3.5 and 4.8 μm can be identified with the unresolved core detected at 2.2 μm (Marco et al. 1997; Thatte et al. 1997; Rouan et al. 1998), itself found to be coincident with the mid-infrared emission peak at 12.4 μm (Braatz et al. 1993), the radio source

S1 (Gallimore et al. 1996a, b) and the center of symmetry of the UV polarization map (Capetti et al. 1995). This strengthens considerably the interpretation of the core infrared emission originating from hot/warm dust in the immediate surroundings of the central engine.

4.2. The torus-like structure at 3.5 and 4.8 μm

The location, position angle and extension of the P.A. $\sim 100^\circ$ structure are strongly suggestive of a dusty/molecular torus. The two bright spots on the edges of the structure outline the “disky” nature of the torus, up to a radius of ~ 40 pc from the central engine. This dusty/molecular torus would be responsible for the collimation of UV radiation from the central engine, leading to the ionizing cone (Pogge 1988; Evans et al. 1991). The overall spatial extension of the torus is found to be ~ 80 pc at 3.5 and 4.8 μm , while it appears to be slightly smaller at 2.2 μm , ~ 50 pc. Under the very simple assumption of optically thick grey-body dust radiation (Barvainis 1987), it is well understood that the emission at 2.2 μm traces hotter dust ($T \sim 1300$ K) than the emission at 4.8 μm ($T \sim 600$ K). The observed difference in size would then signal the existence of a temperature gradient of the grains across the torus.

4.3. The North South extended emission

The NS extended emission (overall extent $\sim 3''$ down to faint emission levels) is also detected at 2.2 μm on a similar scale (Rouan et al. 1998) and at 10 and 20 μm on a larger scale, although along a similar P.A. (Alloin et al. 1999). This structure can be related to the emission of hot/warm dust associated with NLR clouds identified in the northern side of the ionization cone from HST data (Evans et al. 1991) and hidden behind the disc of the galaxy in its southern side. Additional local heating processes, e.g. related to shocks induced by the jet propagation, might be at work as well along the NS extension. The latter suggestion stems from the conspicuous change of direction of the emission at 3.5 μm , following that of the radio jet. Indeed, Kriss et al. (1992) have shown through the analysis of line emission that in NGC 1068 the emitting gas in the NLR is partly excited through shocks triggered by the radio jet.

5. Fluxes, SED and variability

The spectral energy distribution (SED) of the central region of the AGN is an essential parameter in the modeling. To derive this quantity, spatial resolution is obviously needed to disentangle the different sources of emission – dust, stars, non-thermal source.. – and, in that respect, AO observations bring precious informations.

Fluxes at 3.5 and 4.8 μm have been measured through circular apertures centered on the near-infrared peak, with a radius varying from 0.3'' to 1.5'' (22 to 100 pc). They are

depicted in Table 2. A weak PAH line emission at $3.3 \mu\text{m}$ has been detected as well, although no flux calibration is available for this observation, unfortunately.

The aperture flux density as a function of radius, over the region $22 \text{ pc} \leq r \leq 100 \text{ pc}$, can be fitted with a power law: we find $F_L \propto r^{-1.05}$ and $F_M \propto r^{-1.00}$ (where the flux unit is Jy/arcsec^2).

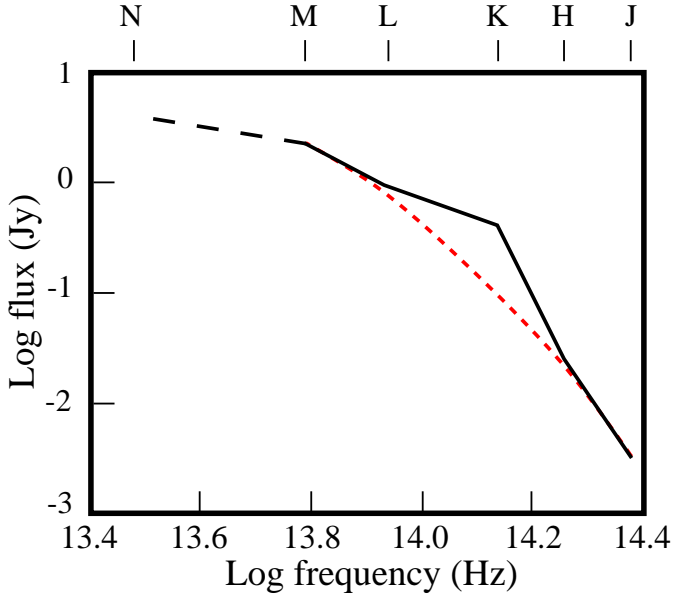


Fig. 2. SED of the central $0.6''$ diameter core (the value for the N band is given for $0.8''$, hence the dashed line between the M and N bands). The dotted line represents an interpolation for establishing the lower-limit of the dust contribution in the K band.

From the set of AO images (this paper and Rouan et al. 1998), as well as high resolution images obtained at $10 \mu\text{m}$ (Alloin et al. 1999), we have reconstructed the SED of the core emission through an $0.6''$ diameter diaphragm, as shown in Fig. 2. Therefore, this SED refers only to the central engine and its immediate environment (including the inner parts of the dusty/molecular torus as well as some contribution from the NS extended structure). In this plot, the contribution from the stellar component has been removed in the J and H bands, following the spatial profile analysis performed by Rouan et al. (1998), while this is not the case in the K band. The part of the near-infrared to mid-infrared emission which is arising from hot to warm dust grains can be represented by a series of grey-bodies of different temperatures and this summation is expected to result in a smooth distribution. Yet, an emission bump at $2.2 \mu\text{m}$ is observed, which could be interpreted as the unremoved stellar contribution in the K band, within the $0.6''$ diameter diaphragm. Under this assumption, an upper limit of 75% for the stellar contribution to the flux at $2.2 \mu\text{m}$, can be derived. This upper limit remains far larger than the 6% effectively derived by

Thatte et al. (1997) within a $1''$ diameter diaphragm, on the basis of the dilution of the equivalent width of a CO absorption feature arising from cold stars.

In any case, a revision of the AGN modeling for NGC 1068 should incorporate the 1 to $10 \mu\text{m}$ SED derived for the innermost region around the central engine and therefore less affected by dilution from other surrounding components (in particular cleaned from the stellar contribution).

It is interesting as well to compare these 1996/1997 measurements in the infrared to those performed by Rieke & Low as early as 1975. Therefore, we have derived, for their $3''$ diameter diaphragm, the 1996/1997 observed fluxes at $1.25, 1.65$ (both uncorrected for the stellar contribution), $2.2, 3.4, 4.8$ and $10 \mu\text{m}$, from Rouan et al. (1998), from the current data set and from Alloin et al. (1999).

Before examining the temporal behavior of the near-infrared emission in NGC 1068, the 1997 flux measurements in the K band can be compared to previous determinations. We consider again a $3''$ diameter diaphragm and compare the 1997 AO measurement to classical photometric measurements. Generally those are performed through much larger diaphragms. However Penston et al. (1974) provide a full set of measurements through diaphragms ranging from $12''$ to $2''$ diameter. Leaving aside the measurements from this paper which have been flagged down for bad transparency or other flaws, we obtain the K magnitude offset when one moves from a $12''$ diaphragm to a $3''$ diaphragm, $\Delta K = 0.85$. This magnitude offset is not expected to vary with time because it refers to the outer parts of the AGN ($r > 110 \text{ pc}$). Then, from the $12''$ diameter diaphragm measurements by Glass (1995), who analyzed the variability properties of NGC 1068, we can infer/extrapolate the K magnitude at the date of the AO measurement by Rouan et al. (1998): $K = 6.81$. Applying the magnitude offset computed above between the $12''$ and $3''$ diameter diaphragms, we predict that the K magnitude should be of 7.66 at the date of the Rouan et al. (1998) observation, while the K magnitude measured is of 7.26 . This agreement is quite satisfactory, given the rather large error-bars involved in the Penston et al. (1974) data set which was obtained more than 25 years ago.

A comparison of the fluxes within a $3''$ diameter diaphragm at both epochs, 1975 (Rieke & Low 1975) and 1997 (this paper) is depicted in Table 3. One notices immediately that a flux increase has occurred over this time interval: by a factor 2 between 2.2 to $4.8 \mu\text{m}$, and by a factor 1.2, at $10 \mu\text{m}$. According to the independent photometric monitoring by Glass (1997), the L band ($3.5 \mu\text{m}$) flux has doubled in 18 years, from 1974 to 1992: our result is in very good agreement with his finding.

Because of the possibly complex way through which the UV-optical photons illuminate and heat the dust grains (direct and/or indirect illumination via scattering on the mirror to the N of the central engine or on dusty regions further out, Miller et al. 1991), it is not possible to

Table 3. Comparison of the infrared fluxes (given in Jy) at two epochs in a 3" diameter diaphragm

	J	H	K	L	M	N
1997	0.13	0.3	0.8	3.4	9.7	21.5
1975			0.3	1.7	5.3	17.9

infer the size of the dust component from light-echo effects acting differentially in the near-infrared and mid-infrared bands.

6. Colors, dust temperature and mass of dust

Following Barvainis (1987), we assume the emissivity of the grains to depend on wavelength as $\lambda^{-1.6}$ and we use a simple model of optically thick grey-body dust emission: $\nu^{1.6} B_\nu(T_{gr})$.

In the general situation of an AGN, the grain temperature varies strongly with distance to the central engine, following a power law (Barvainis 1987): $T_{gr}(r) = 1650 L_{UV,46}^{0.18} r^{-0.36}$ K, where $L_{UV,46}$ is the UV luminosity in units of 10^{46} ergs $^{-1}$ and r the radial distance in parsecs.

6.1. Color gradients in the near-infrared

6.1.1. Colors of the core

Owing to our limitation in spatial resolution in the M band (FWHM = 0.33"), we can measure at best the [L-M] and [K-L] colors of the core through an 0.6" diameter diaphragm centered on the near-infrared emission peak. We find [L-M] = 1.6 ± 0.4 and [K-L] = 1.8 ± 0.2 . It must be noticed however that the contribution of stellar light in the K band (Thatte et al. 1997) has not been removed at this stage and that the observed [K-L] color does not relate only to the dust emission.

6.1.2. Colors of the extended structure

As for the colors of the sources forming the extended structures, and again because of different spatial resolutions in the K, L and M bands, we have considered the mean colors in a ring which extends from $r = 0.3''$ to $r = 0.5''$. This ring does include the emitting regions forming the extended structures along the two directions P.A. $\sim 100^\circ$ and NS, at 3.5 and 4.8 μm , but excludes in part the secondary peaks which delineate the extended structures at 2.2 μm . Therefore, at 2.2 μm , the ring includes more of the diffuse contribution possibly related with the stellar core analyzed by Thatte et al. (1997). The colors found for the ring, representative of a mean 0.4" radius, are [L-M] = 1.6 ± 0.4 and [K-L] = 2.8 ± 0.2 .

6.2. Dust temperature

The advantage of interpreting the [L-M] color is that the L and M band flux contributions are known to arise almost entirely from the dust component. Within the limitation in spatial resolution from the M band data set, we do not detect any [L-M] color gradient within the central 1" region of NGC 1068.

Under the simple assumption of optically thick grey-body emission from the dust component, the observed [L-M] color corresponds to a grain temperature $T_{gr} \sim 480$ K. The foreground extinction to the core has been calculated by several authors (Bailey et al. 1988; Bridger et al. 1994; Efstathiou et al. 1995; Young et al. 1995; Veilleux et al. 1997; Glass 1997; Thatte et al. 1997; Rouan et al. 1998) and an estimate of $A_v \sim 30$ mag is retained. Applying a correction for such an extinction, we deduce an intrinsic color [L-M] = 0.8 ± 0.4 and $T_{gr} \sim 700$ K. The absolute luminosity $L_{UV,opt}$ of the AGN in NGC 1068 – assumed here to be the unique heating source of the dust grains in the AGN environment – can be approached only indirectly and is still quite uncertain. From the analysis by Pier et al. (1994) who have examined various methods for deriving the absolute luminosity of the AGN in NGC 1068 and summarize the current knowledge on this question, we deduce $L_{UV,opt} = 4 \cdot 10^{44}$ erg s $^{-1}$. However it should be noted that this figure has been obtained assuming a reflected light fraction $f_{refl} \sim 0.01$, while the consideration of ionized gas in regions further out inside the ionization cone (ENLR) leads to a value $f_{refl} \sim 0.001$ (Bland-Hawthorn et al. 1991). Then a value as high as $L_{UV,opt} = 4 \cdot 10^{45}$ erg s $^{-1}$ should be envisaged as well. In addition, most of these estimates have been derived without taking into account the fraction of UV-optical flux which provides the dust grains heating: already the K magnitude of the innermost core (FWHM = 0.12"), 9.3, corresponds to an energy output of $\sim 8 \cdot 10^{41}$ erg s $^{-1}$. It might be important to consider the energy radiated in the near- to mid-infrared bands for the evaluation of $L_{UV,opt}$. In conclusion, the figures currently available for $L_{UV,opt}$ in NGC 1068 might be lower limits.

Still, under the simple model of optically thick grey-body dust emission, reaching $T_{gr} \sim 480$ K at $r = 28$ pc requires $L_{UV,opt} = 8 \cdot 10^{45}$ erg s $^{-1}$, a value roughly consistent with the highest figure given above for $L_{UV,opt}$ in NGC 1068. This figure goes up to $L_{UV,opt} = 6.5 \cdot 10^{46}$ erg s $^{-1}$ if the grain temperature is of 700 K at $r = 28$ pc (extinction-corrected estimate), pushing NGC 1068 to the limit between AGN and quasars. This question certainly deserves further attention and above all the consideration of a more elaborated model of the dust region, with regard to its geometry and heating. This is beyond the scope of the current paper and will be discussed in the future.

The [K-L] color in the extended structures can be contaminated by some stellar contribution in the 2.2 μm band. From grains at $T_{gr} \sim 480$ K, which are the dominant contributors, we expect a [K-L] $_{dust}$ color of 4.0. Given the

observed [K-L] value, we deduce that the percentage of the flux at $2.2 \mu\text{m}$ which arises from the dust component (with at most $T_{gr} \sim 480 \text{ K}$) is of 30%. For this estimate, we have not considered any correction for extinction.

How can the lack of [L-M] color gradient between the $0.6''$ diameter core and the extended structures be explained? Given the unresolved and intense core emission at $2.2 \mu\text{m}$ (FWHM = $0.12''$ from Rouan et al. 1998) it can be inferred that the hottest dust grains are extremely confined and located at a radius less than 4 pc. With $L_{UV,opt} = 8 \cdot 10^{45} \text{ erg s}^{-1}$, they would be present only up to $r = 1.1 \text{ pc}$. Hence, there must exist a very steep dust temperature gradient close to the central heating source. Such a few parsec scale corresponds to a resolution which is well beyond that accessible at $3.5 \text{ \& } 4.8 \mu\text{m}$. In fact the L and M emission we are measuring in an $0.6''$ diameter core is already strongly dominated by the warm grains. Because of this suspected steep temperature gradient, the procedure applied previously to derive the stellar contribution in the $0.3''$ to $0.5''$ radius ring cannot be used in the core.

6.3. Mass of the hot dust

The mass of dust associated with the near-infrared emission can be estimated only in a rough way, as it depends on the (unknown) grain composition and grain size distribution. Assuming graphite grains and following Barvainis (1987), the infrared spectral luminosity of an individual graphite grain is given by: $L_{\nu,ir}^{gr} = 4\pi a^2 \pi Q_{\nu} B_{\nu}(T_{gr}) \text{ ergs s}^{-1} \text{ Hz}^{-1}$ where a is the grain radius, $Q_{\nu} = q_{ir} \nu^{\gamma}$ is the absorption efficiency of the grains, and $B_{\nu}(T_{gr})$ is the Planck function for a grain temperature T_{gr} . Following Barvainis (1987), we take $a=0.05 \mu\text{m}$ and in the near-infrared, $q_{ir} = 1.4 \times 10^{-24}$, $\gamma = 1.6$ leading to $Q_{\nu}=0.058$ (for the K band).

Because no [L-M] color gradient is detected towards the $0.6''$ diameter core, we consider the simple case of 2 populations of dust grains in that region, hot grains at $T=1500 \text{ K}$ and warm grains at $T=500 \text{ K}$, matching the extreme values in that region. Solving the equation $F_{\nu,measured} = xF_{\nu,1500 \text{ K}} + yF_{\nu,500 \text{ K}}$ for the three bands available, K, L and M, one derives $2 \cdot 10^{45}$ and $9 \cdot 10^{47}$, for the number of grains at 1500 K and 500 K respectively, in the $0.6''$ diameter core. This indicates that there are ~ 450 times more warm dust grains than hot dust grains in the $0.6''$ diameter core. The warm dust grains dominate the [L-M] color. With a grain density $\rho=2.26 \text{ g cm}^{-3}$, the mass of warm dust grains is found to be $M(\text{warm dust}) \sim 0.5 M_{\odot}$. This mass is above that of hot dust grains detected in two Seyfert 1 nuclei: $0.05 M_{\odot}$ in the case of NGC 7469 (Marco et al. 1998) and $0.02 M_{\odot}$ in the case of Fairall 9 (Clavel et al. 1989). This result supports the fact that only a small fraction of the dust present in the torus is heated close to its sublimation temperature.

7. Grain number density in the warm dust

In NGC 1068, like in other AGN (see for instance NGC 7469), dust is present also in the NLR region (see Fig. 1). It has been shown in Sect. 5 that the infrared emission in the L & M bands over the region $22 \leq r \leq 100 \text{ pc}$ follows a power-law. In addition the temperature of the grains deduced from the [L-M] color has been found to remain roughly constant with radius. Thus, we can derive the radial profile of the warm grain number density in the NLR region, $\eta(r) \propto r^{-\beta}$. Under optically thin conditions, probably applicable in the NLR, the brightness is directly proportional to the grain number density. Then the observed brightness power-law leads to $\beta=1.0$, suggesting a concentrated grain distribution (a uniform grain density would correspond to $\beta=0$). In NGC 7469, the warm dust component led to a figure for β around 1.5 (Marco et al. 1998).

8. Comparison with thick tori model predictions

Several torus models have been developed so far to explain the obscuration of the BLR and UV/X-ray continuum sources along some lines of sight (AGN unification scheme). Some of these models are generic, while others have been designed to match the case of NGC 1068.

Pier & Krolik (1992a, b, 1993) propose a thick, parsec-scale, uniform density torus illuminated by a nuclear source. The dust can be heated up to the effective temperature of the nuclear radiation at the inner edge of the torus. They investigate models with effective temperatures between 500 K and 2000 K . Such a model can explain the unresolved core observed at $2.2, 3.5$ and $4.8 \mu\text{m}$ with AO in the particular case of NGC 1068. Does it explain the extended near infrared emission also revealed by these observations? Indeed, extended emission over $1''$ to $2''$ could result from reflected radiation from the torus and/or dust in the NLR. Therefore, this model accounts for most of the features unveiled with high resolution imaging in the near infrared.

Efstathiou & Rowan-Robinson (1995) propose a model with a very thick tapered disk. They assume the melting temperature of all dust grains to be identical (1000 K), but consider a radial distribution of the grain physical parameters (size and chemical composition). In the case of NGC 1068, Efstathiou et al. (1995) have shown that the torus emission alone cannot account for the total infrared emission. They attribute the excess infrared emission to a distribution of optically thin dust with $\beta=2$ in the NLR region. Their model is in disagreement with the steep grain temperature gradient across the torus, which we infer to exist close to the central engine. Conversely, the dust postulated to be present in the NLR by their model is indeed detected with the AO data set.

Granato & Danese (1994) and Granato et al. (1996, 1997) developed a simple thick ($\tau_e > 30$) torus model extended over several hundreds pc. To minimize the number

of free model parameters, they have adopted a dust density distribution constant with radial distance from the nuclear source. But, they do not rule out the possibility, in the case of smaller values of the optical depth ($\tau_e=1.5$), that a more concentrated density distribution exist. Their predicted size and shape for the near infrared emission are compatible with those derived through AO observations at 2.2, 3.5 and 4.8 μm .

A revised modeling of the AGN in NGC 1068 is timely, owing to the emergence of sub-arcsec resolution images in the near infrared (AO techniques) and in the millimeter range (interferometric techniques), giving direct access to the dust and molecular environment of the central engine.

9. Conclusion

The observation, for the first time at high angular resolution, of NGC 1068 at 3.5 and 4.8 μm provides new informations to build a more realistic model of this AGN under the current unification scheme.

As regard to the AGN structure, we do observe:

- (i) an unresolved core, already known at 2.2 μm to have a size (FWHM) less than 8 pc, and interpreted as the inner region of a dusty/molecular torus in which the central engine of NGC 1068 is embedded,
- (ii) along P.A. $\sim 100^\circ$, an extended emission up to 40 pc on either side of the core, particularly prominent at 4.8 μm . This structure, also detected at 2.2 μm up to 20 pc on either side of the core, is coincident in P.A. with the parsec-scale disc of ionized gas detected with VLBI (P.A. $\sim 110^\circ$), and is found to be roughly perpendicular to the axis of the ionization cone in NGC 1068. We interpret it as the trace, up to a 40 pc radius, of this dusty/molecular torus seen edge-on,
- (iii) an extended emission along the NS direction up to 50 pc from the core and with rather symmetrical properties on either side, both at 3.5 and 4.8 μm . Again, this extended emission is detected, both at 2.2 μm on a similar scale, and at 10 and 20 μm on a slightly larger scale. It reveals the presence of dust in the NLR, heated both by hard radiation within the ionizing cone and by shocks associated with the AGN radio jet.

As regard to the dust temperature and dust distribution in the central arcsec of the nucleus, we get a final picture as follows. As close as $r \sim 1$ pc from the central engine, the dust is heated up to its evaporation temperature, 1500 K. Then the dust temperature declines very rapidly and reaches $T \sim 500$ K at $r < 28$ pc. The total mass of warm dust within a 22 pc radius region is found to be around $0.5 M_\odot$.

It is observed as well that the near infrared flux of NGC 1068, in the 2.2 to 4.8 μm range, has increased by a factor two over some 20 years, while in the 10 μm window the flux increase is only by a factor 1.2.

Our results bring observational evidence of a dusty torus in the AGN of NGC 1068. They further support AGN

modelling in the framework of the unification scheme: a thick torus surrounding a central engine (black hole and accretion disc). Although several models of the AGN in NGC 1068 are available, none matches in detail all the aspects of the current near-infrared results obtained at a subarcsec scale. Such new observational constraints make it both timely and exciting to run updated models. Yet, we are aware that the most convincing and undisputable argument for the presence of the torus-like structure will come from a study of the kinematics of the gas within the 100 central parsec of NGC 1068. We expect such information to be soon obtained from ISAAC/ANTU observations on Paranal.

Acknowledgements. We warmly thank J.P. Veran and E. Gendron for useful discussions, F. Lacombe for his help on the data reduction and Z. Tsetanov for his precious contribution in deriving the HST composite image seen by the WFAS. We acknowledge as well precious comments from an anonymous referee.

References

- Alloin D., Marco O., 1997, *Ap&SS*, 248, 237
- Alloin D., Pantin E., Lagage P.O. et al., 1999, *A&A*, in prep.
- Antonucci R.R.J., Miller J.S., 1985, *ApJ*, 297, 621
- Bailey J., Axon D.J., Hough J.H., Ward M.J., McLean I., et al., 1988, *MNRAS*, 234, 899
- Barvainis R., 1987, *ApJ*, 320, 537
- Beuzit J.L., Hubin N., Gendron E., et al., 1994, *SPIE* 2201
- Bland-Hawthorn J., Sokoloski J., Cecil G., 1991, *ApJ*, 375, 78
- Braatz J.A., Wilson A.S., Gezari et al., 1993, *ApJ*, 409, L5
- Bridger A., Wright G.S., Geballe T.R., 1994, in *Infrared Astronomy with Arrays: the next generation*, McLean Eds., p. 537
- Capetti A., Macchetto F., Axon D.J., Sparks W.B., Boksenberg A., 1995, *ApJ*, 452, L87
- Chapman S., Walker G., Morris S., 1999, in *Proceedings of the ESO/OSA Sonthofen Topical Meeting on Astronomy with Adaptive Optics*, 7-11 Sept. 1998, ed. D. Bonaccini, ESO, p. 73
- Chelli A., Perrier C., Cruz-Gonzales I., Carrasco L., 1987, *A&A*, 177, 51
- Clavel J., Wamsteker W., Glass I.S., 1989, *ApJ*, 337, 236
- Efstathiou A., Hough J.H., Young S., 1995, *MNRAS*, 277, 1134
- Efstathiou A., Rowan-Robinson M., 1995, *MNRAS*, 273, 649
- Evans I., Ford H., Kinney, A., et al., 1991, *ApJ*, 369, L27
- Gallimore J.F., Baum S.A., O'Dea C.P., Pedlar A., 1996a, *ApJ*, 458, 136
- Gallimore J.F., Baum S.A., O'Dea C.P., Brinks E., Pedlar A., 1996b, *ApJ*, 462, 740
- Glass I., 1991, *MNRAS*, 276, L65
- Glass I., 1997, *Ap&SS*, 248, 191
- Granato G.L., Danese L., 1994, *MNRAS*, 268, 235
- Granato G.L., Danese L., Franceschini A., 1996, *ApJ*, L11
- Granato G.L., Danese L., Franceschini A., 1997, *ApJ*, 147
- Kriss G.A., Davidsen A.F., Blair W.P., Ferguson H.C., Long K.S., 1992, *ApJ*, 394, L37
- Krolik J., 1999, in *Active Galactic Nuclei*, Princeton Series in Astrophysics, Princeton University Press

- Lacombe F., Marco O., Geoffray H., et al., 1997, *PASP*, 110, 1087
- Lynds R., Faber S.M., Groth E.J., et al., 1991, *ApJ*, 369, L31
- Marco O., Alloin D., Beuzit J.L., 1997, *A&A*, 320, 399
- Marco O., Alloin D., 1998, *A&A*, 336, 823
- Miller J.S., Goodrich R., Mathews W., 1991, *ApJ*, 378, 47
- Penston M.V., Penston M.J., Selmes R.A., Becklin E.E., Neugebauer G., 1974, *MNRAS*, 169, 357
- Pier E.A., Antonucci R., Hurt T., Kriss G., Krolik J.H., 1994, *ApJ*, 428, 124
- Pier E.A., Krolik J.H., 1992a, *ApJ*, 399, L23
- Pier E.A., Krolik J.H., 1992b, *ApJ*, 401, 99
- Pier E.A., Krolik J.H., 1993, *ApJ*, 418, 673
- Pogge R., 1988, *ApJ*, 328, 519
- Rieke G., Low F., 1975, *ApJ*, 199, L13
- Rouan D., Rigaut F., Alloin D., et al., 1998, *A&A*, 339, 687
- Thatte N., Quirrenbach A., Genzel R., Maiolino R., Tecza M., 1997, *ApJ* 490, 238
- Veilleux S., Goodrich R.W., Hill G.J., 1997, *ApJ*, 477, 631
- Young S., Hough J.H., Axon D.J., Bailey J.A., Ward M.J., 1995, *MNRAS*, 272, 513